J Mater Sci: Mater Med (2009) 20:591–595
DOI 10.1007/s10856-008-3585-0

Bactericidal properties of $ZnO–Al_2O_3$ composites formed from layered double hydroxide precursors

Yan-Jun Lin · Xiang-Yu Xu · Lei Huang · David G. Evans · Dian-Qing Li

Received: 21 January 2007 / Accepted: 4 September 2008 / Published online: 14 October 2008

Abstract $ZnO–Al_2O_3$ composites with different Zn/Al molar ratios (*R*) have been prepared using zinc–aluminium layered double hydroxides (LDHs) $Zn_RAl–CO_3$ as precursor. The samples were characterized by XRD, ICP, EDX, EPR and FT-IR. The results show that ZnO is highly dispersed in all of the $ZnO–Al_2O_3$ composites. Bactericidal experiments against *Staphylococcus aureus* ATCC 6538 and *Bacillus subtilis* var. *niger* ATCC 9372 were carried out by contacting the bacteria and spores with the $ZnO–Al_2O_3$ composites. The composites all showed high bactericidal activity against *Staphylococcus aureus* ATCC 6538, and the bactericidal efficiency against *Bacillus subtilis* var. *niger* ATCC 9372 increased with increasing content of ZnO. The mechanism of bactericidal activity of $ZnO–Al_2O_3$ has also been investigated. It is suggested that highly active O_2^- and •OH species generated on the surface of $ZnO–Al_2O_3$ particles react with the peptide linkages in the cell walls of bacteria or spores resulting in their destruction.

1 Introduction

Solid bactericidal materials have been widely studied and applied because of their excellent bactericidal activity and structural stability. Work by Sawai and his coworkers [1–4] showed that metal oxides such as ZnO have strong bactericidal activity and capability, especially against gram-positive bacteria. It is desirable to devise protocols for the preparation of ZnO with a highly dispersed structure, because the bactericidal properties of ZnO prepared by ordinary processes can be reduced by particle agglomeration effects.

Layered Double Hydroxides (LDHs) are a type of layered anionic clay. The identities and relative amounts of cations in the layers and interlayer counterions in LDHs can be varied widely [5–9]. The LDHs structure is based on $M(OH)_6$ octahedral units which share edges to form brucite-like layers. These octahedral units contain M^{2+} and M^{3+} ions and the unit containing M^{3+} ion is positively charged. These positive octahedral units tend to keep away from each other because of electrostatic repulsion, which results in the metal ions being highly dispersed within the layers. Mixed metal oxides with high specific surface area and having a high degree of dispersion of metal cations can be prepared by calcination of LDHs precursors. In our previous work, a series of $Mg_RAl–CO_3$–LDHs (where *R* represents the Mg/Al molar ratio) were prepared by different methods and calcined at 500°C to afford the corresponding oxide composites, in which MgO was highly dispersed. The resulting materials showed excellent bactericidal efficacy against *Staphylococcus aureus* and *Bacillus subtilis* var. *niger* [10]. Since Al_2O_3 is known to lack any bactericidal activity [4], the improvment in bactericidal properties can be attributed to the high degree of dispersion of MgO on the support.

In this work, a series of $Zn_RAl–CO_3$–LDHs (where *R* represents the Zn/Al molar ratio) have been prepared by a method involving separate nucleation and aging steps (SNAS) [11]. Highly dispersed $ZnO–Al_2O_3$ composites with different contents of ZnO were prepared by calcination of these $Zn_RAl–CO_3$LDHs precursors. The effects of varying the dispersion state of ZnO on the bactericidal properties

Y.-J. Lin · X.-Y. Xu · L. Huang · D. G. Evans · D.-Q. Li (✉)
State Key Laboratory of Chemical Resource Engineering, Beijing University of Chemical Technology, Beijing 100029, People's Republic of China
e-mail: lidq@mail.buct.edu.cn

against *S. aureus* ATCC 6538 and *B. subtilis* ATCC 9372, together with the bactericidal mechanism, have been investigated and the results are discussed in this paper.

2 Experimental

2.1 Experimental materials

$Zn(NO_3)_2 \cdot 6H_2O$, $Al(NO_3)_3 \cdot 9H_2O$, NaOH, Na_2CO_3 and urea were all A.R. grade reagents. Water was deionized, with electric conductivity less than 10^{-6} S cm^{-1}. *Bacillus subtilis* var. *niger* (spore, ATCC 9372) and *Staphylococcus aureus* (bacterium, ATCC 6538) were obtained from the Chinese Center for Disease Control and Prevention in form of slice packages according to international standards, with bacteria or spore number of 10^6 cfu in each piece (cfu = colony forming units).

2.2 Preparation of ZnO–Al_2O_3 composites based on LDHs precursors

Mixed salt solutions containing Zn^{2+} and Al^{3+} (with Zn/Al molar ratios of 2, 2.5, 3, 3.5 and 4) were prepared with the concentration of Zn^{2+} fixed at 0.8 mol l^{-1}. A mixed alkali solution containing NaOH and Na_2CO_3 was prepared with $n(OH^-)/[n(Zn^{2+}) + n(Al^{3+})] = 1.6$ and $n(CO_3{}^{2-})/n(Al^{3+}) = 2.0$. Following the SNAS method, these two solutions were simultaneously added to a reactor (a modified colloid mill) [12] and mixed for 2 min. The resulting suspensions were aged at 60°C for 6 h and dried at 70°C for 24 h. The Zn_RAl–CO_3–LDHs precursors were calcined at 500°C (with a temperature ramping rate of 10°C min^{-1}) for 4 h to give ZnO–Al_2O_3 composites with Zn/Al molar ratios of 2, 2.5, 3, 3.5 and 4.

2.3 Preparation of nano-ZnO comparative sample

A zinc carbonate hydroxide precursor was prepared by mixing aqueous solutions of $Zn(NO_3)_2 \cdot 6H_2O$ and urea at 100°C for 3 h according to a procedure in the literature [13]. The precursor was filtered and washed, followed by drying at 70°C for 12 h and calcination at 500°C for 3 h to afford the nano-ZnO sample.

2.4 Bactericidal testing

Bactericidal activity was determined according to the Chinese National Standard GB15981-1995 (evaluating methods and standards for the efficacy of disinfection and sterilization). After being heated at 120°C for 20 min, ZnO–Al_2O_3 composites or nano-ZnO were placed in a sterile conical flask, to which was added 50 ml phosphate buffer (pH 6.8) followed by 0.5 ml germ or spore mixture (10^5 cfu ml^{-1}). After the mixture was mechanically shaken for 24 h at 37°C, an aliquot (0.5 ml) of the liquid mixture was placed on a sterile plate with a general germ culture medium and cultured for 48 h at 37°C. The surviving colonies were counted by eye with the help of a magnifier and the bactericidal efficacy was calculated according to the following formula:

$$\text{bactericidal efficacy}(\%) = \frac{\textit{alive} \text{ number in reference group} - \textit{alive} \text{ number in experiment group}}{\textit{alive} \text{ number in reference group}} \times 100\%$$

The tests were carried out five times with each ZnO–Al_2O_3 composite and nano-ZnO, using both *B. subtilis* ATCC 9372 and *S. aureus* ATCC 6538 and the average values of bactericidal efficacy were calculated.

2.5 Analysis and characterization

Powder X-ray diffraction (PXRD) patterns were recorded on a Shimadzu XRD-6000 X-ray powder diffractometer (Cu K_α radiation, $\lambda = 0.15406$ nm) between 3° and 90°. The scan speed was 5° min^{-1}. Elemental analysis (Zn, Al) was carried out using a Shimadzu ICPS-7500 inductively coupled plasma emission spectrometer (ICP-ES). Scanning electron microscopy (SEM) (with energy dispersive spectroscopy) was carried out using a Hitachi S-530 instrument. Electronic paramagnetic resonance (EPR) spectra were recorded at room temperature on a Bruker EPR 500 spectrophotometer working at $v = 9.5$ GHz. FT-IR spectra were recorded on a Bruker Vector 22 FT-IR spectrometer (as KBr discs, with a weight ratio of sample to KBr of 1:100).

3 Results and discussion

3.1 Preparation of ZnO–Al_2O_3 composites

The powder XRD patterns of the Zn_RAl–CO_3–LDHs precursors ($R = 2$, 2.5, 3, 3.5 and 4) (Fig. 1) show the

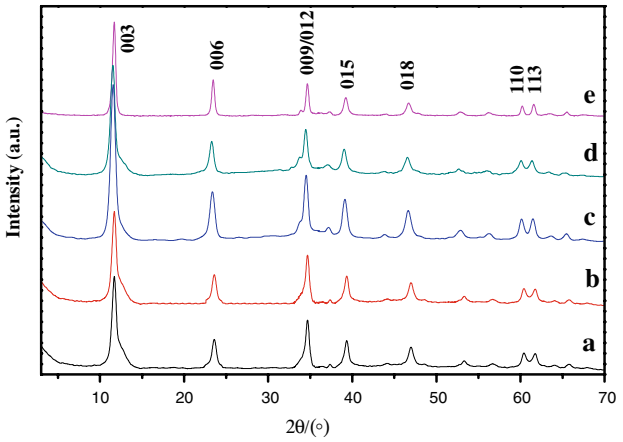

Fig. 1 Powder XRD patterns of $Zn_RAl–CO_3–LDHs$ with Zn/Al molar ratios $R = 2$ (**a**), 2.5 (**b**), 3 (**c**), 3.5 (**d**) and 4 (**e**)

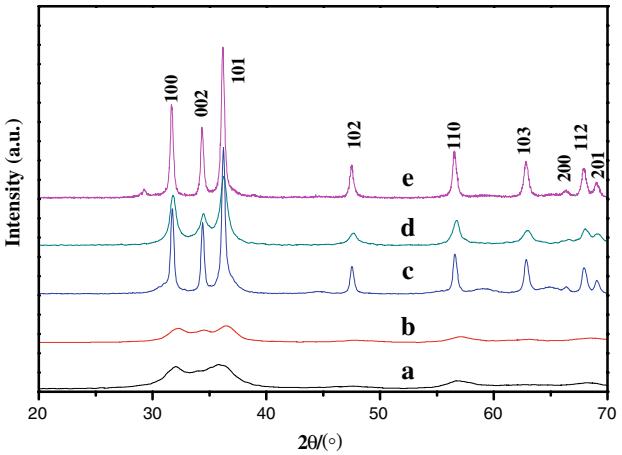

Fig. 2 Powder XRD patterns of $ZnO–Al_2O_3$ with Zn/Al molar ratios $R = 2$ (**a**), 2.5 (**b**), 3 (**c**), 3.5 (**d**) and 4 (**e**)

Table 1 Indexing of XRD patterns for $Zn_RAl–CO_3–LDHs$ with $R = 2$, 2.5, 3, 3.5 and 4

Zn/Al molar ratio before mixing	d_{003}/(nm)	d_{110}/(nm)	Cell parameter a/(nm)	Cell parameter c/(nm)
2.00:1.00	0.7570	0.1531	0.3062	2.2710
2.50:1.00	0.7579	0.1536	0.3072	2.2737
3.00:1.00	0.7659	0.1538	0.3076	2.2977
3.50:1.00	0.7676	0.1534	0.3068	2.3028
4.00:1.00	0.7683	0.1541	0.3082	2.3049

Table 2 ICP analysis data for $ZnO–Al_2O_3$

Zn/Al molar ratio before mixing	$[Zn^{2+}]$/(μg ml^{-1})	$[Al^{3+}]$/(μg ml^{-1})	Zn/Al molar ratio in samples
2.00:1.00	49.696	10.202	2.01:1.00
2.50:1.00	46.264	7.886	2.42:1.00
3.00:1.00	42.085	5.585	3.13:1.00
3.50:1.00	44.085	5.123	3.55:1.00
4.00:1.00	41.656	4.062	4.26:1.00

characteristic reflections of LDHs materials [14]. The cell parameters a and c can be calculated from the positions of the (110) reflection and the basal (00l) reflections, respectively [15]. As listed in Table 1, the cell parameter a shows a slight increase with decreasing amount of Al^{3+} in the host layers because the radius of Zn^{2+} (0.74 Å) is larger than that of Al^{3+} (0.50 Å); the cell parameter c also increases due to decreasing electrostatic attraction between the host layers and the guest anions.

Figure 2 shows the powder XRD patterns of $ZnO–Al_2O_3$ composites obtained by calcination of $Zn_RAl–CO_3–LDHs$ ($R = 2$, 2.5, 3, 3.5 and 4) at 500°C for 4 h. The intensities of the Bragg reflections assigned to the ZnO phase increase with the Zn/Al ratio. Elemental analysis results for the $ZnO-Al_2O_3$ composites listed in Table 2 are in close agreement with the metal ratios in the initial synthesis mixtures.

3.2 Dispersion of Zn and Al in $ZnO–Al_2O_3$ composites

The $ZnO–Al_2O_3$ composite with Zn/Al molar ratio of 3 was further investigated. Qualitative analysis scans for elemental Zn and Al by EDX are displayed in Fig. 3. The distributions of dots in the figures show that both elements are highly dispersed. Such high dispersion can be ascribed to the characteristics of the precursors. In the $Zn_RAl–CO_3–LDHs$ system, partial replacement of Zn^{2+} cations by Al^{3+} cations in the host layers produces a net positive charge and Al^{3+} cations tend to keep away from each other in the host layers due to the unfavorable electrostatic repulsion which would result between adjacent Al^{3+} cations. When the layered structure collapses on calcination, the positions of the metal cations along the a direction remain essentially unchanged. Therefore, ZnO nano-particles formed by calcination are highly dispersed due to the separation effects of the small Al_2O_3 particles.

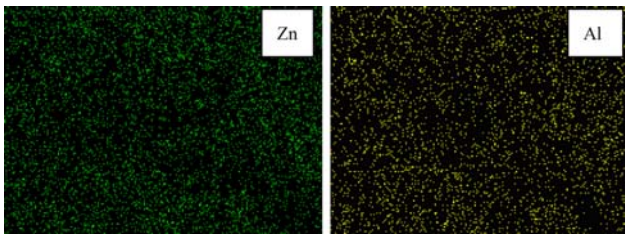

Fig. 3 Energy dispersive X-ray microanalysis (EDX) of Zn and Al in the $ZnO–Al_2O_3$ composite with Zn/Al molar ratio of 3

Table 3 Bactericidal efficacies of ZnO–Al_2O_3 composites and ZnO

Zn/Al molar ratio	SA/ (m^2 g^{-1})	Bactericidal efficacy against *S. aureus* ATCC 6538/(%)	Bactericidal efficacy against *B. subtilis* ATCC 9372/(%)
2.00:1.00	62.4	99.9	81.7
2.50:1.00	66.2	99.9	83.4
3.00:1.00	76.5	99.9	86.2
3.50:1.00	81.2	99.9	87.7
4.00:1.00	82.2	99.9	88.3
ZnO	34.7	99.9	77.8

3.3 Effect of ZnO content in ZnO–Al_2O_3 composites on bactericidal ability

Staphylococcus aureus ATCC 6538 is a ubiquitous bacterium in nature with adverse effects on human health. *B. subtilis* ATCC 9372 is a type of spore with a compact cell wall and strong resistance against chemical agents. The bactericidal efficiencies of the ZnO–Al_2O_3 composites and pure ZnO (ca. 50 nm particle size) against both bacteria and spores were investigated by contact for 24 h. ZnO nano-particles are known to produce free electrons and positive cavities in the presence of water and air under radiation by sunlight or ultraviolet [2]. Spores are killed by interaction with O_2^- and •OH, which are produced from O_2 excited by positive cavities. As listed in Table 3, the bactericidal efficiency of 0.50 g nano-ZnO against *S. aureus* ATCC 6538 can reach 99%, while against *B. subtilis* ATCC 9372 it is only 77%. The bactericidal efficiency of ZnO–Al_2O_3 composites containing 0.50 g ZnO is above 99% against *S. aureus* ATCC 6538. The bactericidal efficiency against *B. subtilis* ATCC 9372 exceeds 88% for a high ZnO content in ZnO–Al_2O_3, although Al_2O_3 has no bactericidal activity [4]. Thus the enhanced bactericidal efficiency can be attributed to the high dispersion of nano-ZnO in the ZnO-Al_2O_3 composites which results in a larger number of active sites of nano-ZnO being exposed on the surface. Therefore, more O_2^- and •OH species can be produced giving excellent bactericidal performance. The number of active sites increases with the amount of ZnO in the ZnO–Al_2O_3 composites leading to enhanced bactericidal efficiency, as long as the amount of ZnO is not too high to result in extensive phase segregation and agglomeration of particles.

3.4 Preliminary studies of the mechanism of bactericidal activity of ZnO–Al_2O_3 composites

The EPR spectrum of the ZnO–Al_2O_3 composite with Zn/Al molar ratio of 3 recorded at room temperature is shown in Fig. 4. The strong EPR signal at $g = 1.96$ has been attributed to shallow donors and its position appears to be independent of the shallow-donor identity [16, 17]. Many authors have assigned this EPR signal to the singly ionized oxygen vacancy Vo^+ [18, 19]. Oxygen has a strong tendency to adsorb on metal oxide surfaces, acting as an electron acceptor. Adsorbed O_2 can capture electrons from the conduction band forming superoxide ions (O_2^-).

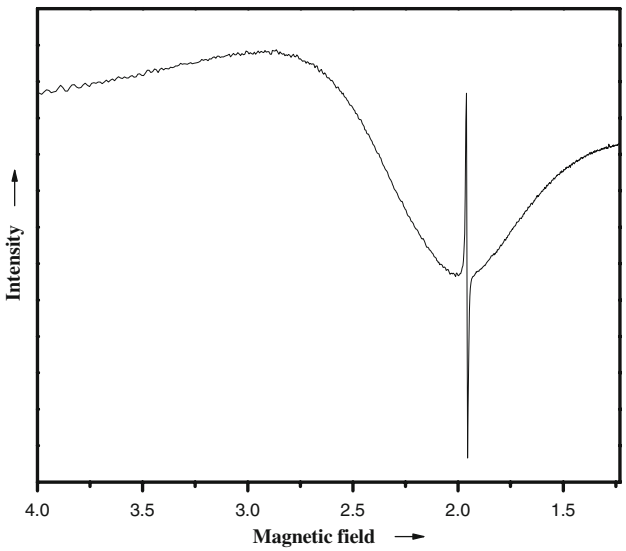

Fig. 4 Room temperature EPR spectrum of the ZnO–Al_2O_3 composite with Zn/Al molar ratio of 3

Figure 5 shows the FT-IR spectra of *B. subtilis* ATCC 9372 and the ZnO–Al_2O_3 composites with Zn/Al molar ratio of 4 before and after reaction with *B. subtilis* ATCC 9372. For *B. subtilis* ATCC 9372 (shown in Fig. 5a), the proteins in the cell walls of the spores contain many peptide linkages. The strong peak at 2886 cm^{-1} corresponds to the C–H stretching vibration in $–CH_2CO–$ groups. Another

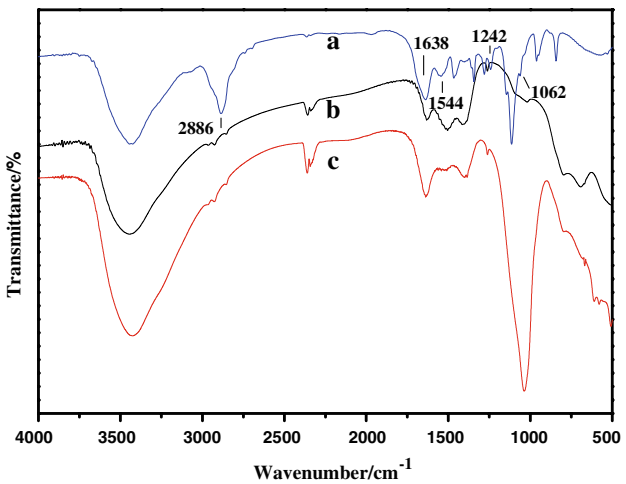

Fig. 5 FT-IR spectra of *B. subtilis* ATCC 9372 (**a**), ZnO–Al_2O_3 composite (**b**) and mixture of ZnO–Al_2O_3 composite and *B. subtilis* ATCC 9372 (**c**)

strong peak at 1638 cm^{-1} is characteristic of the carbonyl stretching vibration of secondary amides such as peptides. The N–H deformation peak is located at 1544 cm^{-1}, and the weak peak at 1242 cm^{-1} is due to the C–N stretching vibration. After contact of ZnO–Al_2O_3 composites with the spores, the resulting mixture was dried at low temperature followed by mixing with KBr and the corresponding FT-IR spectra were recorded. As shown in Fig. 5c, the carbonyl stretching peak is still visible, but the intensity of the C–O stretching vibration at 1062 cm^{-1} increases markedly, suggesting that the positive carbon atom in the C=O moiety has been attacked by O_2^- and •OH formed as a result of the presence of ZnO in the ZnO–Al_2O_3 composites. The original C–N bond in the peptide is transformed into an alkylamine and the cell walls of the spores are destroyed in this way.

4 Conclusions

ZnO–Al_2O_3 composites with Zn/Al molar ratios of 2, 2.5, 3, 3.5 and 4 have been prepared by calcination at 500°C of Zn_RAl–CO_3–LDHs prepared using a method involving separate nucleation and aging steps (SNAS). ZnO in the ZnO–Al_2O_3 composites is highly dispersed, as shown by EDX, due to the structural characteristics of the precursor Zn_RAl–CO_3–LDHs.

Owing to the high dispersion of nano-ZnO in ZnO–Al_2O_3 composite samples, the bactericidal efficiencies against *S. aureus* ATCC 6538 can reach 99%. Furthermore, the bactericidal efficiencies of the ZnO–Al_2O_3 composites against *B. subtilis* ATCC 9372 are superior to pure nano-ZnO and increase with amount of ZnO in the composite.

The O_2^- and •OH produced by ZnO in the ZnO–Al_2O_3 composites react with –NH–CO– bonds resulting in the destruction of the cell walls. As a result, the ZnO–Al_2O_3 composites show excellent bactericidal performance.

Acknowledgments This work was supported by the National Natural Science Foundation of China (Grant No. 20631040) and the Natural Science Foundation of Beijing (Grant No. 2062017).

References

1. J. Sawai, H. Kojima, F. Kano, H. Igarashi, A. Hashimoto, E. Kawada, T. Kokugan, M. Shimizu, World J. Microb. Biot **14**, 773 (1998)
2. O. Yamamoto, J. Sawai, T. Sasamoto, Int. J. Inorg. Mater. **2**, 451 (2000)
3. O. Yamamoto, Int. J. Inorg. Mater. **3**, 643 (2001)
4. J. Sawai, J. Microbiol. Meth. **54**, 117 (2003)
5. F. Cavani, F. Trifiro, A. Vaccari, Catal. Today **11**, 173 (1991)
6. D.G. Evans, X. Duan, Chem. Commun. **7**(5), 485 (2006)
7. D.G. Evans, R.C.T. Slade, Struct. Bond. **119**, 1 (2006)
8. J. He, M. Wei, B. Li, Y. Kang, D.G. Evans, X. Duan, Struct. Bond. **119**, 89 (2006)
9. X.R. Jiang, F. Li, D.G. Evans, X. Duan, Acta Chim. Sin. **62**, 16 (2004)
10. L. Huang, D.Q. Li, D.G. Evans, X. Duan, Eur. Phys. J. D **34**, 321 (2005)
11. Y. Zhao, F. Li, D.G. Evans, X. Duan, Chem. Mater. **14**, 4286 (2002)
12. X. Duan, Q. Z. Jiao (2000) Chinese Patent, CN00132145. 5
13. X.C. Shi, S. Wang, Y.H. Qin, S.W. Wei, J. Wang, New Chem. Mater. **31**, 32 (2003)
14. L. Zou, F. Li, X. Xiang, D.G. Evans, X. Duan, Chem. Mater. **18**, 5852 (2006)
15. V.R.L. Constantino, T.J. Pinnavaia, Inorg. Chem. **34**, 883 (1995)
16. R.M. Espí, G. Jeschke, I. Lieberwirth, C.M. Gómez, G. Wegner, J. Phys. Chem. B **111**, 697 (2007)
17. A.B. Djurišić, W.C.H. Choy, V.A.L. Roy, Y.H. Leung, C.Y. Kwong, K.W. Cheah, T.K.G. Rao, W.K. Chan, H.F. Lui, C. Surya, Adv. Funct. Mater. **14**, 856 (2004)
18. P.H. Kasai, Phys. Rev. **130**, 989 (1963)
19. A. Pöppl, G. Völkel, Phys. Status Solidi. A **115**, 247 (1989)